Coupling of drift, diffusion, and electroconvection, in the vicinity of growing electrodeposits

V. Fleury, J.-N. Chazalviel, and M. Rosso
Laboratoire de Physique de la Matière Condensée, Ecole Polytechnique, 91128 Palaiseau, France
(Received 8 March 1993)

We propose a theoretical approach to the problem of electroconvection in the vicinity of electrodeposits which are growing in quasi-two-dimensional cells. Charges at the tips of the branches are expected to induce a convective motion of the solution. We show theoretically that, in the steady state, pairs of contrarotative vortices must be expected between neighboring branches. The concentration map is explicitly derived in the limit where diffusion is negligible, as compared to drift and convection. A more realistic concentration map is computed numerically in the case of nonnegligible diffusion. We compare the theoretical predictions to experimental observations of the growth of copper deposits from a solution of copper sulphate. We show that both the convective vortices and the concentration gradient are very well described by the theoretical model. Hence the simple theoretical approach that we present gives a good understanding of the intricate problem of the electroconvective, diffusive, and drift motion of the ions. To our knowledge, an electrodeposition model which incorporates these three aspects has not been published previously.

PACS number(s): 68.70.+w, 82.45.+z, 47.65.+a, 81.15.Lm

I. INTRODUCTION

Electrochemical deposition (ECD) of ramified metallic clusters in thin cells, without supporting electrolyte, has attracted much attention in the last decade because of its possible relationship with the diffusion-limited-aggregation (DLA) algorithm proposed by Witten and Sander [1,2]. The DLA numerical simulation shows that one should expect a fractal morphology when the growth of a cluster is ruled by a Laplacian field. The first experimental electrochemical clusters which were reported have been claimed to be fractal, and fairly well described by DLA [3]. Their growth was believed to be governed by a Laplacian field, which was thought to be either the diffusion field or the electric field.

However, it was soon recognized that in most experimental conditions using an unsupported binary electrolyte (e.g., copper sulfate, zinc sulfate) the clusters are rather dense or dendritic than fractal [4,5]. In the case of the dense morphology (DM) the clusters are formed of many almost rectilinear branches whose tips have a smooth envelope. As a consequence, the description of the growth must go beyond a Laplacian field. A stabilization mechanism was proposed [6] to account for the observed smooth envelope. While this model may hold, from the point of view of linear stability analysis, it does not describe the actual motion of the ions in the vicinity of the deposit. Moreover, the validity of this model has been questioned recently [7].

In order to get a better understanding of the ramified deposition mechanism, many experimental investigations have been performed [8–21]. Many parameters were explored, such as salt formula, cell geometry, concentration of the solution, applied potential, or electric field etc. While getting deeper into the details of the growth process it has been realized that the genuine electrochemical aspects of the growth were not irrelevant, and that ECD may not belong at all to the DLA class of structures which is already well known [22]. The main weakness of the DLA model when applied to ECD is that DLA is basically a single-field model (the concentration gradient), while three fields (at least) are present in ECD (the cation and anion concentration gradients in addition to the electric field).

An electrochemical model [22] describing the interplay of these three fields was proposed for the growth of ramified clusters (in two-dimensional rectangular cells and without supporting electrolyte). This model will be recalled in some detail in Sec. II. Its most striking prediction is that the growth speed of the deposit is simply the speed at which the anions withdraw ahead of the tips of the deposit while the deposit is growing. This has been verified experimentally [11,16]. However, the prediction for the concentration map is not in agreement with the experimental observations. It is in fact necessary to incorporate convection in the description of the growth, the fluid velocity being one more field which should be added to the three fields mentioned above. One possible source of fluid motion is the electroconvection (or "Coulomb" convection) due to the positive charges which are expected to be found in the fluid in the vicinity of the tips. In this article, we will show theoretically that electroconvection should indeed be expected in the vicinity of the tips (Sec. III). Then, we will derive the flow pattern around the deposits, for the case of a dense morphology (Sec. IV).

Taking these results into account, we will give an analytical description of the ionic motion in the vicinity of branches when neglecting diffusion (Sec. IV). This limiting case will help us understanding the role of electroconvection, and prompt us to perform a numerical calculation of the concentration gradients in the vicinity of the branches, in the presence of diffusion (Sec. V). The concentration profiles will be shown as a function of the

diffusion constant D.

We will turn to the experiments in Sec. VI. We will show that electroconvective motion exists between the branches, by using small oil droplets in the solution. In spite of many sources of noise and randomness, the observed vortices are very well described by the calculated ones. We will present experimental observations of the concentration gradients by an interferometric method, whose results are at variance with other observations from the literature [20,21]. The concentration gradients we report on exhibit an archlike shape between two branches, which is in agreement with our theoretical predictions.

II. THE MODEL WITHOUT CONVECTION

Chazalviel has proposed an analytical and numerical description of ECD without a supporting electrolyte [22]. The model predicts the existence of a positively charged zone and of a large electric field near the cathode. These two factors will be responsible for the convective motion, as will be proved in Sec. III. Before proceeding to the next sections, we need to recall how the charges and potential distributions are predicted in Chazalviel's model. This description of ECD goes through two steps, which we now recall in some detail.

A. Deposition on a flat smooth cathode

Suppose a constant potential difference U_a is set between a linear cathode (at potential zero) and a linear anode (at potential U_a), in a thin electrochemical cell, filled with a salt of a metal, for example, copper sulphate ($Cu^{2+}SO_4^{2-}$) (see Fig. 1). The equations which govern the ECD are

$$\frac{\partial C_c}{\partial t}=D_c\Delta C_c-\mu_c\mathbf{E}\cdot\mathrm{grad}C_c-\mu_c C_c\mathrm{div}\mathbf{E}\ , \tag{1}$$

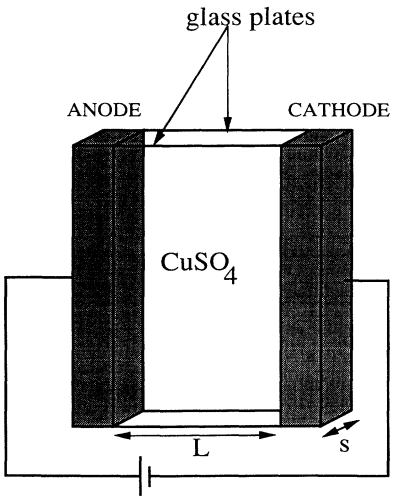

FIG. 1. Sketch of the electrochemical cell. A current is imposed between two linear electrodes. The thickness of the cell is of the order of 0.1 mm, the distance between electrodes is of the order of 2 cm, and the length of the electrodes is of the order of 6 cm.

$$\frac{\partial C_a}{\partial t}=D_a\Delta C_a+\mu_a\mathbf{E}\cdot\mathrm{grad}C_a+\mu_a C_a\mathrm{div}\mathbf{E}\ , \tag{2}$$

$$\mathrm{div}\mathbf{E}=e(z_cC_c-z_aC_a)/\epsilon\epsilon_0\ , \tag{3}$$

where D's are diffusion constants, C's concentrations, and μ's mobilities; the subscript a stands for anion and the subscript c stands for cation. z_c and z_a are the charge numbers of the cations and of the anions, respectively. $\mathbf{E}$ is the electric field, $-e$ the charge of the electron, ϵ the dielectric constant of the solvent, and ϵ_0 the vacuum permittivity.

In this first step, the cations are expected to form a smooth deposit on the cathode, with no treelike structures. The cathode remains flat during this stage of ECD, so one can restrict the equations to the x direction and obtain

$$\frac{\partial C_c}{\partial t}=D_c\frac{\partial^2 C_c}{\partial x^2}-\mu_cE\frac{\partial C_c}{\partial x}-\mu_cC_c\frac{\partial E}{\partial x}\ , \tag{4}$$

$$\frac{\partial C_a}{\partial t}=D_a\frac{\partial^2 C_a}{\partial x^2}+\mu_aE\frac{\partial C_a}{\partial x}+\mu_aC_a\frac{\partial E}{\partial x}\ , \tag{5}$$

$$\frac{\partial E}{\partial x}=e(z_cC_c-z_aC_a)/\epsilon\epsilon_0\ . \tag{6}$$

The steady state resulting from this set of equations is determined analytically and numerically in Ref. [22]. It appears that while the applied electric field tries to bring the cations toward the cathode and the anions toward the anode, a charged layer starts forming in the vicinity of the cathode (Fig. 2). There is a depletion of both cations and anions near the cathode, but the balance of the charges shows an excess of positive charges. This excess of positive charges is essentially found near the cathode, and is responsible for the strong curvature of the potential. A minute excess of positive charges will also be found in the bulk of the cell, where $\partial E/\partial x$ will be weakly positive. Hence two zones can be distinguished in the cell (Fig. 3), a charged layer (CL) near the cathode, and a quasineutral region (QNR) which occupies the rest of the cell. Notice that the overall neutrality of the solution is not conserved, and that it becomes slightly positive.

The potential just outside the CL starts from zero when the potential is switched on, and rises while the excess of positive charges increases near the cathode (Fig. 2). Eventually, the potential outside the CL reaches a value close to U_a. The thickness x_1 of the CL is of the order of a few micrometers in usual experimental conditions. Hence, in the case of smooth deposition, the potential difference which is set between the electrodes is, at the end, almost totally absorbed by the CL located very near the cathode. There is still a very small potential gradient in the QNR, such that the drift motion of the anions cancels with the diffusion:

$$D_a\mathrm{grad}C_a/C_a+\mu_a\mathbf{E}=0\ , \tag{7}$$

so the anions do not participate in the current through the cell. This is sensible, and comes from the fact that the anions are neither produced nor deposited during the

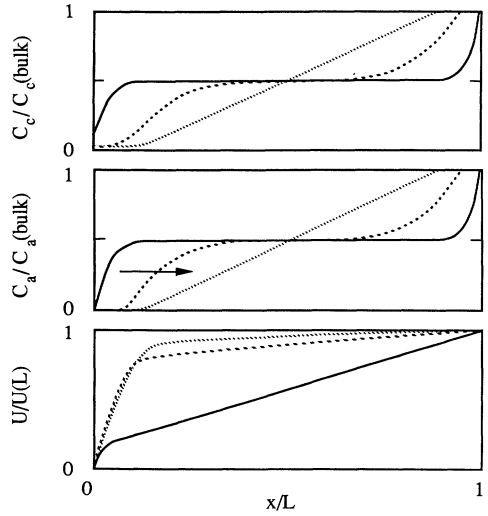

FIG. 2. The concentration of cations and of anions that would be found at different stages of growth of a smooth deposit on the cathode (solid line: $t=10^2$ s; dashed line: 10^3 s; dotted line: 10^4 s), and the potential difference (bottom). As one notices, the potential near the cathode increases progressively. A large field appears near the cathode. An excess of positive charges forms in a thin layer near the cathode, which is responsible for the curvature of the potential. The bulk of the solution is quasineutral. Here, due to irrealistically small concentrations ($C=10^{11}$ cm^{-3}), the charged layer appears thick. In usual conditions, its thickness is very small, of the order of a few micrometers.

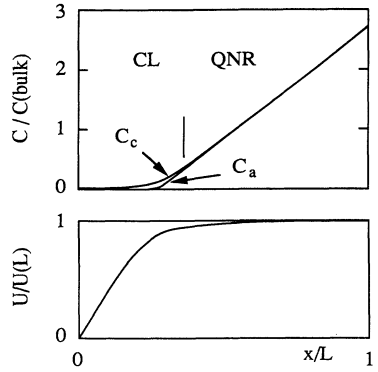

FIG. 3. The potential and the concentration through the cell, in the case of smooth deposition, when the steady state is achieved. Irrealistically small values of the concentration are used ($C=10^{10}$ cm^{-3}), so that the two zones can be clearly distinguished. There is a charged layer (CL) near the cathode, where an excess of cations and a large field are found. The rest of the cell is quasineutral (QNR), but there remains a very small excess of positive charges.

ECD. Conversely, the motion of the cations is the sum of a diffusive motion and a drift motion:

$$\mathbf{v}_c=-D_c\text{grad}C_c/C_c+\mu_c\mathbf{E} \tag{8}$$

which, taking into account Eq. (7), becomes

$$\mathbf{v}_c=-D_c\text{grad}C_c/C_c-(\mu_c/\mu_a)D_a\text{grad}C_a/C_a\ , \tag{9}$$

since z_aC_a is almost equal to z_cC_c in the QNR, this last equation may be written

$$\begin{aligned}\mathbf{v}_c&=-[D_c+(\mu_c/\mu_a)D_a]\text{grad}C_c/C_c\\&=-D_c(1+z_c/z_a)\text{grad}C_c/C_c\ .\end{aligned} \tag{10}$$

This shows that the motion of the cations is very slow, being governed essentially by diffusion. The current will be limited to small values of the order of 100 μA/cm^2. In the QNR, the concentrations are roughly equal and vary linearly:

$$z_cC_c=z_aC_a=2[(x-x_1)/L]C_\infty\ , \tag{11}$$

where C_∞ is the common initial (uniform) value of z_cC_c and z_aC_a. [Note that the grad$C$ terms in Eqs. (7) and (8) are simply constant.]

The distinction between the CL and the QNR will be of upmost importance in the derivation of the Coulomb force, in Sec. III. (This model of ECD, which would describe deposition before branch formation, has been calculated independently by Bruinsma and Alexander [23].)

B. Step two: Growth of branches

In fact, the potential $U(x_1)$ which will be found outside the CL cannot rise to its maximum possible value U_a, because the huge electric field in the vicinity of the branches will provoke instabilities, such as dendritic growth or convective motion, which will either roughen the cathode, thus changing the limiting conditions, or modify the set of equations themselves, by adding another transport mechanism, or both. It has been shown experimentally [16,19,24] that in a first transient regime the potential $U(x_1)$ reaches a critical value δU (similar to the η parameter of Ref. [11]) much smaller than U_a. While the exact value of δU has not yet been predicted theoretically, it has been shown experimentally to be of the order of 1 V [16,19,24]. The experimental evolution of the electrochemical parameters during this first stage of growth, where the set of equations (1)–(3) holds, has been shown to be very well fitted by the model described above [24,25].

The potential drop δU is found at the tips of the branches during growth, and remains constant. It is associated to a limiting value of the electric field near the tips, above which the structuring of the branches is possible. As shown in Refs. [16,19,22], a steady state of growth can only be achieved in parallel geometry using constant current conditions, instead of constant potential. In the latter case, branches form and grow at a constant rate. A numerical solution has been obtained, which gives the concentration maps around a comb of branches which grow steadily. In this calculation, the fluid is supposed to be at rest so the set of equations (1)–(3) is assumed to hold. Typical concentration maps are displayed in Ref. [22], Fig. 4.

While it has not been possible to calculate an analytical formula for the concentration maps in two dimensions around the teeth in the most general situation, it is still

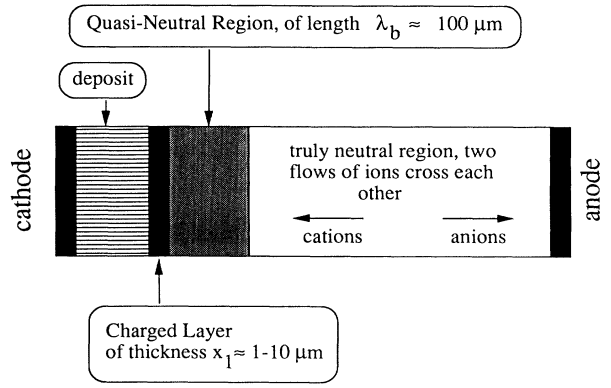

FIG. 4. Schematic view of the ion distribution in the cell, during the growth of the branches, in the limit of very small spacing between the branches. One successively finds a charged layer near the tips, over a distance of a few micrometers, then a quasineutral region, over a typical distance of 100 μm, then a truly neutral region where the two ionic species simply cross each other (drawing not to scale).

possible to derive the expression giving the potential drop associated with the excess positive charge, and of the thickness of the charged layer, as functions of the distance to the tips, in the limiting case of an infinitely small spacing between the teeth. These are

$$U=\delta U[1-(1-x/x_1)^{3/2}] , \tag{12}$$

$$C_c=\left[-\frac{\epsilon\epsilon_0 E_\infty C_\infty(1+\mu_a/\mu_c)}{2z_c^2 e(x_1-x)}\right]^{1/2} , \tag{13}$$

where

$$x_1=\left[\frac{9\epsilon\epsilon_0\delta U^2}{-8eE_\infty C_\infty(1+\mu_a/\mu_c)}\right]^{1/3} \tag{14}$$

is the thickness of the charged layer which is found in the vicinity of the tips, and E_∞ is the field in the bulk. This is akin to modeling the deposit as a flat growing sheet instead of a comb. It also shares obvious analogies with the case of ECD on a smooth motionless cathode which was explained previously. Especially, there still exists a CL near the moving front of the branches, and a QNR in a region of thickness λ_b, where λ_b is the backstream diffusion length:

$$\lambda_b=-(kT/eE_\infty)(z_c+z_a)[z_c z_a(1+\mu_a/\mu_c)]^{-1} .$$

In practical cases λ_b is of the order of 100 μm, which is much larger than x_1. In the rest of the cell, there is a truly neutral region where the two flows of ions of equal concentration simply cross each other (see Fig. 4). In the frame of the laboratory the growth speed of the deposit is the speed at which the anions withdraw from the vicinity of the deposit, and it is written as

$$\mathbf{v}_a=-\mu_a\mathbf{E}_\infty . \tag{15}$$

The CL and the QNR advance in the cell with the tips of the branches while the truly neutral zone shrinks.

While the limit of infinitely small spacing is of little interest for an accurate description of the growth, it enables one to derive the strength of the Coulomb force which acts on the liquid, as it will be shown now.

III. DISCUSSION OF THE EXISTENCE OF ELECTROCONVECTION

It has been known for long that as soon as a charged liquid is placed in an electric field, a Coulomb force will act on the charges, and hence on the liquid. Many examples of electroconvective motion appear in the literature [26–32]. Experiments, and theories, have been proposed for the case of electroconvection of a dielectric liquid submitted to unipolar injection of charges. In these experiments and theories, a controlled distribution of charges is supposed to be created (by thermal effects, or by means of ionic pumps), in the liquid near an electrode. Then the motion of the charged liquid, submitted to an electric field, is studied. For large enough electric fields, convective transport plays an important role. However, the case of a unipolar injection of charges, while worth being mentioned, is rather different from the case we are discussing, in which two carriers are present in the solution ("binary electrolyte"), whose concentrations depend on the electric field as described in Sec. I. The question whether electroconvective motion of the solution would appear in the conditions of fast electrochemical deposition has only been addressed very recently [23,33]. After deriving a model for deposition along a smooth interface in a steady solution, which is essentially identical to the model described above (Sec. II), Bruinsma and Alexander [23] have studied the convection which could be expected from the concomitant existence of a positive excess of charges and of an electric field. The conclusion of these authors is that electrohydrodynamic convection must be expected, but that this effect is very small, and could easily be hidden by, for example, gravity-driven convection. We will now show that, while the calculations performed by these authors are valid and help in understanding electroconvection in general, they do not apply to convection around the ramified electrochemical deposits.

As we can see from the model described in Sec. I, the volume force that acts on the liquid [which is equal to $(z_c C_c - z_a C_a)eE$] can be formally divided into two contributions: the contribution of the CL and the contribution of the QNR, as long as these two zones exist. The charge and the field in the CL are both very large, but the thickness of the CL is very small (of the order of micrometers). The charge in the QNR is very small and the field is very small, but this region is large, since it fills all the cell in the case of smooth deposition and spreads over a distance λ_b (100 μm) in the case of ramified deposition. What will be the essential condition to the convective motion? It is argued by Bruinsma and Alexander that the contribution of the CL is strictly zero, on the argument that the electric force on the liquid is oriented towards the electrode (Fig. 5), which is the wrong way for destabilization. This means that the electric force acting on the liquid near the electrode is a stabilizing one. In the context of Rayleigh-Bénard convection, it would correspond to driving the

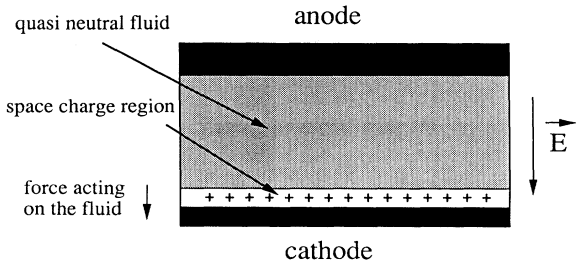

FIG. 5. Scheme of the cell, before branch formation, and without convection. Bruinsma and Alexander argue that the charged layer cannot provoke convective motion because the convective force is oriented towards the cathode, which is the stabilizing direction.

liquid located on the bottom of a cell, towards the bottom of the cell. (However, keep in mind that gravity convection with a thermal gradient is very different from electroconvection, because in the case of electroconvection both the charges and the field are determined self-consistently throughout the cell, while gravity is a constant in Rayleigh-Bénard convection). Hence, these authors have only considered the contribution of the QNR to the convective motion. Indeed, their finding is that this contribution is very small, because neutrality is a very good approximation in the quasineutral region (with their values of the parameters the deviation from charge neutrality is of the order of $10^{-12}eC_\infty$, while in our case it is closer to $10^{-10}eC_\infty$).

In fact, the contribution of the CL to the convective motion *cannot* be neglected. Suppose that the deposit has been growing for a while according to the model described in Sec. II B, without convection. We clearly see that the force acting on the liquid will not be stabilizing at all, because instead of a flat compact cathode, the liquid sees an array of ramified and soft branches. The liquid is not simply pressed by the electric force on the cathode: it will try to move between, or even through, the branches. So, as soon as branches have appeared, the argument of Bruinsma and Alexander will not hold any longer. While our argument is valid when branches exist, one may question whether it holds at the very beginning of the growth process. We argue that as soon as the slightest protrusion appears on the cathode, the CL at the tip of the protrusion will exert a destabilizing force.

We now proceed and calculate the force exerted on the liquid in the charged layer. We first start by the limiting case of infinitely small spacing between trees; we show afterwards that the result is extendable to any array of parallel branches by means of simple flux-conservation arguments.

In the CL, the positive excess of charges is almost equal to the concentration of cations given in Eq. (13). The electric field is simply obtained from Eq. (12):

$$E(x)=-(3/2x_1)\delta U(1-x/x_1)^{1/2}\ , \tag{16}$$

so at any point x lying inside the CL, the force $df(x)$ acting on an elementary volume $d\Omega$ of fluid is

$$df(x)=[z_cC_c(x)-z_aC_a(x)]eE(x)d\Omega\ , \tag{17}$$

which, since the concentration of anions is negligible in the CL, reduces to

$$df(x)\approx z_cC_c(x)eE(x)d\Omega\ , \tag{18}$$

replacing $C_c(x)$ and $E(x)$ by their expression [Eqs. (13) and (16)], one finds

$$df(x)\approx(1+\mu_a/\mu_c)E_\infty C_\infty ed\Omega\ . \tag{19}$$

This force is independent of x. when integrating it over the whole charged layer, it is simply found that the force f is

$$f\approx(1+\mu_a/\mu_c)E_\infty C_\infty ex_1sl \tag{20}$$

where l is the length of the electrodes, and s the thickness of the cell. The front exerts on the section of the cell (of area sl) a pressure P equal to

$$P\approx(1+\mu_a/\mu_c)E_\infty C_\infty ex_1\ . \tag{21}$$

An order of magnitude estimate of P, for usual values of the concentration (10^{-2} mol l^{-1}) and the field (10 V/cm), and remembering that the thickness of the charged layer is of order 1 μm, is $P\approx10^3$ Pa. This pressure is very large, and indeed enough to provoke a motion of the fluid. Of course, the branches themselves hinder the motion of the fluid. Also, the force acts only on the charged layer, and nowhere else, so the Navier-Stokes equation must be invoked and solved around a nontrivial boundary: the front of the branches, with a local force acting only inside the CL (this will be treated in greater detail in the next section).

Equation (19) shows that df is independent of x through the CL. This is not surprising. Since the CL is totally depleted of anions, the current is only transported by the cations. The current is the sum of the drift current and of the diffusion current. Diffusion is negligible in the CL because the electric field is very large (of order 10^4 V/cm) hence the current density is written simply as $J=\mu_cez_cC_c(x)E(x)$. This in turn is equal to $\mu_cdf/d\Omega$. Since J is constant, $z_cC_c(x)E(x)$ is equal to $[(\mu_a+\mu_c)/\mu_c]eC_\infty E_\infty$. Remember that in the neutral region C_∞ is simply equal to what it was at the beginning of the growth process, because the neutral region is a region of constant electrochemical parameters which simply shrinks while the deposit grows. The field E_∞ is merely the applied field. The volume force $[(\mu_a+\mu_c)/\mu_c]eC_\infty E_\infty$ has to be integrated over the volume of the charged layer: slx_1. Of course, x_1 depends on δU, which, as stated before, is not known theoretically. The reasoning we have derived in the previous lines is very general, and applies as well to branches separated by a large distance. Since the deposit, in this model, has periodic invariance along the x axis, we can restrict ourselves to a single box of width b containing a single branch. The force on an elementary volume $d\Omega$ very close to the tip is written as

$$\frac{df(\text{tip})}{d\Omega}=ez_cC_c(x,y)E(x,y)\ . \tag{22}$$

The crucial point is that in the vicinity of the deposit the concentration of negative ions is almost zero, so

$$ez_c C_c(x,y)E(x,y)=J(x,y)/\mu_c \ . \tag{23}$$

If we now integrate the force along the cross section Σ of the tip we find that

$$\int \frac{df(\text{tip})}{d\Omega} dS=(1/\mu_c)J(x,y)\Sigma=(1/\mu_c)J_\infty bs \ , \tag{24}$$

where J_∞ is the current density in the neutral region far ahead of the tips. The right-hand side of the last equation comes from the conservation of the flux. Then, the total force acting at the tip is

$$f(\text{tip})=(1+\mu_a/\mu_c)eC_\infty E_\infty bsx_1 \ . \tag{25}$$

Of course, x_1 depends on δU and probably on the specific geometry of the apex of the branch.

Before going to the next section, let us insist on the following points: As soon as one tries to deposit a metal in a thin electrochemical cell, without a supporting electrolyte, one creates a positively charged zone in the vicinity of the cathode. If the branches grow, and still have a smooth envelope, the charged zone will move in the electrolyte with the tips of the branches. The electroconvective force around a single tip can be approximated by Eqs. (23)–(25), which is essentially an exact result, as long as the liquid is at rest. This force is expected to be very large, much larger than the force acting on the quasineutral region. It will exert on the cross section Σ, a pressure equal to $(1+\mu_a/\mu_c)eC_\infty E_\infty(bs/\Sigma)x_1$: As compared to Eq. (21), this value is increased by the factor bs/Σ. Although the value of x_1 may be different here, we expect that this pressure may still be larger than $(1+\mu_a/\mu_c)eC_\infty E_\infty x_1$, given by Eq. (21) in the case of infinitely small spacing between branches.

IV. THE MODEL FOR CONVECTION WHEN DIFFUSION IS NEGLECTED

We have proved in Sec. III that the excess of positive charges which is found in the vicinity of the tips can provoke an electroconvective force on the liquid. We now address the question of the convective pattern that will be found around the deposit, in a steady state. A short version of this has appeared in a Letter [34]. We will rapidly recall the hypotheses, and some results. We will then give a full discussion of the main issues, when neglecting diffusion. Diffusion will be taken into account in the next section.

The simplest way of modeling the deposit [22], in the dense regime, is to consider it as an infinite comb of thin parallel teeth with equal spacing b. The question arises of what will be the behavior of the fluid when arriving on the teeth. One should pay attention to the fact that the deposit is very lacunar at scales below the typical width of a branch. One can refer to the micrographs presented by Hibbert and Melrose in Ref. [12] for a better understanding of the intimate structure of the deposit. It seems obvious that water can flow through the deposit, much like wind blowing through a leafless tree. As a matter of fact the deposit does not push the water ahead. If one considers the (liquid plus deposit) mixture as homogeneous, then the "concentration" of metal in this mixture is $(1+\mu_c/\mu_a)C_\infty$ (C_∞ is usually of order 10^{-2} moll^{-1}). This shows how lacunar it is (compact copper has a density corresponding to 10^2 moll^{-1}). We then make the approximation that the solution will flow freely through the deposit.

Now we must model the distribution of forces. As pointed out in Sec. II, the force acts mainly in the charged layer, which is a very narrow region close to the tip. We make the approximation that the liquid is only driven by this force, and neglect the contribution of the QNR. The force is oriented *anti*parallel to growth and acts on the liquid only when it penetrates into the CL. The width of the CL is very small compared to the distance b between the teeth, which is larger than the thickness of the cell (of order 100 μm). We then model the distribution of forces as an array of Dirac-δ forces acting at the teeth, directed toward negative y and of modulus f (Fig. 6). In order to compute the fluid flow, we consider the cell as almost two dimensional. In the real experiments, the distance between branches will be of order 1–40 times the thickness of the cell. The two-dimensional (2D) approximation is certainly not valid for small spacings between neighboring trees; however, we have not gone beyond the 2D approximation.

Note that the convective motion discussed here is rather different from gravity-driven convection since in the case discussed here the force is not a bulk force, but a local force. Note also that the parameter δU is only known experimentally.

We have solved in Ref. [34] the problem of the motion of the fluid around a moving comb, with the previous hypotheses, in the limit of small Reynolds numbers, and for a Poiseuille flow [35]. This is done in two steps: First, the solution around a single motionless tooth, and then with an array of growing teeth. Let us call Ψ the stream vector [35], which is such that $\Psi=(0,0,\psi(x,y))$, and $\mathbf{v}=\text{curl}\Psi$, where $\mathbf{v}$ is the speed averaged along the direction perpendicular to the cell. (The only nonzero component of Ψ is the z component because, when averaged along z, the flow is two dimensional.) After some simple calculations $\psi(x,y)$ is found to be [34,36]

$$\psi(x,y)=\frac{1}{2\pi}\frac{s}{12\rho\nu}f\frac{x}{r^2} \ , \tag{26}$$

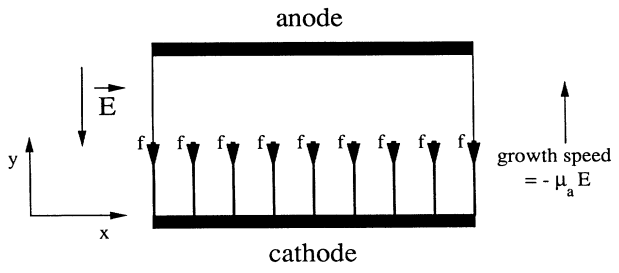

FIG. 6. Scheme of the cell, used as model for the analytical derivation of the fluid flow. The force is supposed to act only at the tips, where the charge is considered as pointlike.

where r is the distance to the tip of the tooth, and ν is the kinematic viscosity (whose unit is $m^2 s^{-1}$, $\rho\nu$ is called the dynamic viscosity). The stream lines are the constant ψ lines. One should note that due to the assumption of infinitely thin teeth, the fluid velocity is infinite at the tip.

The solution for a steady comb is a sum of terms analogous to the one in Eq. (26), corresponding to each tooth:

$$\psi(x,y)=\frac{s}{24\pi\rho\nu}f\sum_{k=-\infty}^{k=+\infty}\frac{x-kb}{r_k^2} \tag{27}$$

(where r_k is the distance to the tip of rank k).

Then the solution for the growing comb is simply obtained, *in the moving frame of the teeth*, by subtracting $v_a=-\mu_a E_\infty$ from the motion of the fluid. This corresponds to adding the term $v_a x$ to $\psi(x,y)$. Finally, the z component of the stream function reads

$$\psi(x,y)=v_a x+\frac{s}{24\pi\rho\nu}f\sum_{k=-\infty}^{k=+\infty}\frac{x-kb}{r_k^2}\ . \tag{28}$$

Now, the flow pattern, of course, will depend on the ratio $\alpha=v_a/(sf/24\pi b^2\rho\nu)$. If the force is negligible, the flow will simply be a laminar flow antiparallel to the growth (in the laboratory frame, the liquid is at rest). We show in Fig. 7 the different aspects of the flow pattern for different values of the ratio α. As one can see, the patterns fall into two classes. Either the closed loops of the two vortices between neighboring teeth touch each other, or they do not. In the first case (small values of α), the liquid coming from ahead will be trapped in a kind of funnel, arrive at the tip, and then leave the tip through a symmetrical kind of funnel. In the second case (large values of α), part of the liquid goes from far ahead to far behind without ever getting close to the tips. In all cases the liquid in the vortices is trapped there and rotates, speeding up as it gets closer to the tips. Let us say in anticipation that the experimentally observed vortex, in the case of dense parallel growth, is of the first kind: the liquid is trapped in a funnel and the neighboring vortices do touch each other. (In the case of fractal growth one cannot model the deposit by a rectilinear comb, and there is no steady state; however, vortices of similar shape are still observed.)

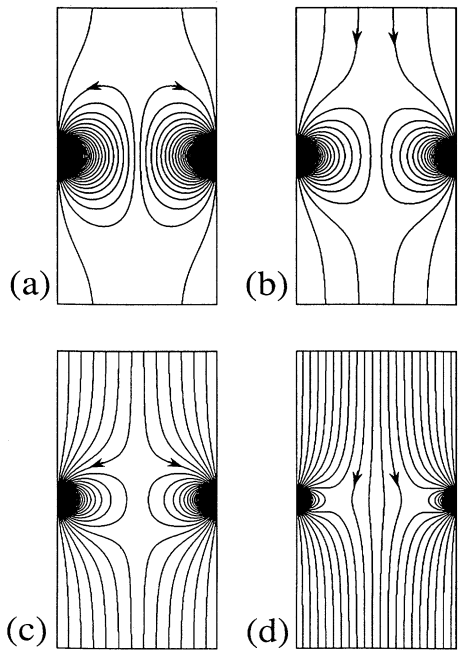

FIG. 7. Fluid patterns around the growing comb, as a function of the parameter α, which represents the ratio of the growth speed over the force. The fluid patterns are shown in the moving frame of the tips. (a) $\alpha=0.25$; (b) $\alpha=2$; (c) $\alpha=6$; (d) $\alpha=20$.

We have been able to derive the fluid flow without considering the actual fate of the anions because the force acting on the fluid was restricted to the local force at the tips. This force is not supposed to depend on the distribution of ions around the comb, in the quasineutral region, but only on the strength of the local force at the tips. As shown in Ref. [34] this simple fluid model allows one to derive an approximate concentration map.

It is known experimentally that the concentrations of both cations and anions are constant and equal to C_c(bulk) and C_a(bulk) in the neutral region, while the concentrations are equal to zero far behind, between the branches [24]. As a consequence, the motion of the ions in the neutral region is only governed by electric drift (the ∇C term is equal to zero). We are interested in the frontier between the two zones, where a concentration gradient must be expected. However, we will suppose in the next paragraphs that diffusion is everywhere negligible (and not only far ahead or far behind), and that the transport of the ions is only governed by convection and electric drift. We will arrive to a rather simple concentration pattern, which, in our opinion, catches the main features of the ionic transport around the deposit. Then, in the next section, diffusion will be incorporated into the model. The case without diffusion will appear as a limiting case of the more general problem in which convection, diffusion, and drift are taken into account altogether.

Whatever the deposition mechanism, we know that the anions are neither produced nor deposited during the electrochemical process: Since their concentration is zero behind the tips, this implies that, in the steady state, they are frozen *in the moving frame* of the tips (in the laboratory frame the two flows of ions cross each other and the anions do participate in the charge transport). Since we restrict ourselves to the case where diffusion is neglected, this requires that $-\mu_a\mathbf{E}+\mathbf{v}=\mathbf{0}$. Therefore, we may expect two zones around the deposit: (1) A zone containing anions (and hence, cations) where $\mu_a\mathbf{E}=\mathbf{v}$. (2) A zone free of anions, and hence of cations, where the actual shape of the electric field is of little importance, as regards the deposition mechanism.

When neglecting diffusion, the frontier between the two zones behaves like a sharp interface (this is where neglecting diffusion seems a rather crude approximation). The border between the two zones must itself be both a field line and a stream line. Indeed, along the border line,

the anions and cations which are present on the concentrated side must cross each other without penetrating into the emptied zone. This can only be achieved if both kinds of ions move tangentially along the borderline. The pattern must then exhibit a stream line which separates the plane into two parts, one which is concentrated, and one which is not. Let us remark that a domain of concentrated region cannot be enclosed into an emptied one because its contour would be a field line making a loop, which is not possible. Then the concentrated region must be connected [37]. Also, we know experimentally that the rear part of the front, between the teeth of the comb, is in the emptied zone. If we now turn to the fluid flow patterns, we see that, among the fluid patterns which we have determined, only the class of patterns for which the vortices touch each other exhibit a stream (and field) line separating the plane into two parts. This line is the arch formed by the largest closed loops of the vortices. It is in fact composed of two stream lines which start from a stagnation point and go in opposite directions. By continuity, the zone containing the ions is necessarily on the upper side. Then, in the moving frame, the two zones mentioned above are as follows: (1) The zone on the upper side of the arch, ahead of the branches, which acts as a funnel for the cations, and in which the anions are frozen (Fig. 8). (2) The lower zone and the vortices themselves, between the branches, which are empty of ions of both kinds.

Now, we can show that the concentration in the concentrated zone is everywhere equal to the bulk concentration: Indeed, since the fluid is incompressible, the flux of $\mathbf{v}$ is conserved, and so is the flux of $\mathbf{E}$. The conservation of the flux of cations implies that the concentration of cations is constant. Neutrality implies that the concentration of anions is constant, and so, equal to C_a(bulk).

The picture of the motion of the ions is then as sketched in Fig. 9: The anions drift backwards in the convective flow, and their drift velocity compensates exactly the flow velocity, in the moving frame. The cations go towards the tips with a speed roughly twice as fast [$(1+\mu_a/\mu_c)$ in fact] as the drift speed. Both ionic species remain in the funnel formed by the fluid and field lines. No ion penetrates into the vortices.

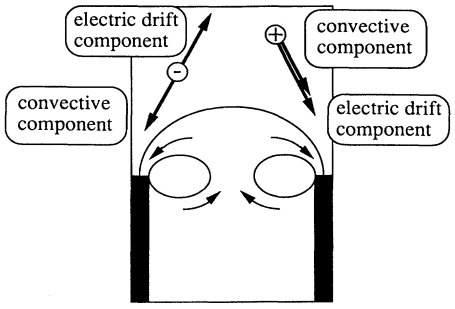

FIG. 9. Schematic motion of the ions in the moving frame of the tips. An anion is shown on the left, and a cation on the right. The anion is frozen because in the moving frame electric drift and convection cancel each other out. On the contrary, electric drift and convection add up for the cation.

The question arises of how it is possible that the field lines should have this shape. One indeed expects the field lines between a comb and a linear anode to be as in Fig. 10(a), and not as in Fig. 10(b), which is the shape of the field which our calculations give. In fact, the arch is a sharp interface between two media of different chemical composition, one of it being in principle an insulator. As it is casual in electrolyte junctions, one should expect a distribution of charges along this arch. This specific distribution of charges along the arch will bring the normal component of the field along the arch to zero. Our model then predicts the existence of charges along the virtual interface between the solution containing ions and the vortices. The convective force that will be added to the problem because of this interfacial distribution of charges is much weaker than the convective force due to the charge at the tips. Indeed, in order to bend the field lines, the areal distribution of charges σ must be of order

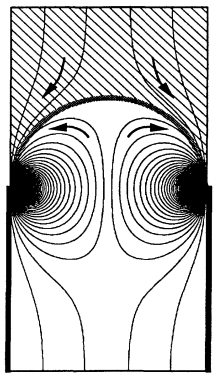

FIG. 8. Concentration and fluid velocity map between two teeth, in the moving frame. $z_c C_c$ and $z_a C_a$ are equal and constant on the upper side of the arch which joins two neighboring teeth (hatched zone). In the steady-state regime, pairs of contrarotative vortices will always be found between the branches. The cations do not penetrate between the branches; they move along the fluid lines until they reach the growing tip. The anions are frozen in the moving frame.

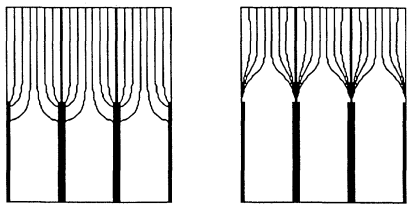

FIG. 10. Electric field lines expected between a comb and a linear anode in normal circumstances (a). Electric field which is necessary in order for the anions to be frozen (b). In this case, the electric field is proportional to the fluid velocity field. Inside the vortices, no ions will be found, so the electric field is *a priori* not known.

$$\sigma \approx \epsilon\epsilon_0 E(\text{arch}) , \tag{29}$$

the field along the arch is of the order of E_∞, so the force ϕ acting on the liquid along the arch (of length $\approx b$) will be of the order of

$$\phi \approx bs\epsilon\epsilon_0 E_\infty^2 . \tag{30}$$

The volume force $df/d\Omega$ inside the charged layer is of order

$$df/d\Omega \approx eC_\infty E_\infty , \tag{31}$$

which has to be integrated over a volume typically equal to sbx_1, so the total force is typically of the order of

$$f \approx eC_\infty E_\infty sbx_1 . \tag{32}$$

The ratio ϕ/f is then of the order of

$$\phi/f \approx \epsilon\epsilon_0 E_\infty / eC_\infty x_1 . \tag{33}$$

An order of magnitude estimate, with $E_\infty = 10$ V/cm, $C_\infty = 10^{-2}$ mol l^{-1}, $e = 1.6\times10^{-19}$ C, $\epsilon\epsilon_0 = 7\times10^{-10}$ F m^{-1}, $x_1 = 10^{-4}$ cm, gives

$$\phi/f \approx 10^{-6} . \tag{34}$$

This shows that the model is self-consistent.

To summarize the simple model that we have presented: (1) There are pointlike charges (and forces) at the tips of the branches; therefore, (2) there exist convective vortices between the tips; (3) there exists a depleted zone below the arches; (4) ahead of the vortices the electric field is proportional to the fluid velocity, in the moving frame; (5) the concentration in the funnel is equal to the bulk concentration; (6) there must be a distribution of charges along the arch, which is a virtual interface.

Before going to the next section, where we shall address the question of diffusion inside the vortices, let us make the following remark: We have considered as an experimental fact that the concentration behind the branches is zero. This was used as a cornerstone for the derivation of the concentration map around the branches. However, one can wonder why the rear zone is totally depleted of ions. It has been argued by Chazalviel [22], in the case of a steady solution, that if some ions penetrate between the branches, this will favor branching, and new branches will form. The same argument holds in the case of a convective flow. We conjecture that if the pattern is of the form which allows penetration of the solution between the branches, then branching will be favored in the rear zone: In the steady state the fluid flow always exhibits the arch between neighboring tips. Of course, the patterns that we have shown stand only for the steady state, and they can only be used as a qualitative hint of how branching will proceed.

V. IONIC TRANSPORT WHEN TAKING INTO ACCOUNT DIFFUSION, CONVECTION, AND DRIFT

A. Qualitative approach to diffusion into the vortices

An exact analytical solution of the ECD process that would incorporate diffusion, convection, and drift seems out of reach. This would require solving the following set of equations around the moving comb:

$$\frac{\partial C_c}{\partial t} + \mathbf{v}\cdot\text{grad}C_c = D_c\Delta C_c - \mu_c \mathbf{E}\cdot\text{grad}C_c - \mu_c C_c \text{div}\mathbf{E} , \tag{35a}$$

$$\frac{\partial C_a}{\partial t} + \mathbf{v}\cdot\text{grad}C_a = D_a\Delta C_a + \mu_a \mathbf{E}\cdot\text{grad}C_a + \mu_a C_a \text{div}\mathbf{E} , \tag{35b}$$

$$\text{div}\mathbf{E} = e(z_c C_c - z_a C_a)/\epsilon\epsilon_0 , \tag{36}$$

coupled to the Navier-Stokes equation:

$$\frac{\partial \mathbf{v}}{\partial t} + \mathbf{v}\cdot\text{grad}\mathbf{v} = \nu\Delta\mathbf{v} - (1/\rho)\text{grad}P + (1/\rho)e(z_c C_c - z_a C_a)\mathbf{E} . \tag{37}$$

However, we can derive qualitatively the thickness of the interface from simple arguments. It is easy to show that the length over which diffusion will spread the interface must vary as $(D/|\nabla\mathbf{v}|)^{1/2}$. Indeed, in the steady-state regime the anions satisfy the following equation:

$$\mathbf{v}\cdot\text{grad}C_a = D_a\Delta C_a + \mu_a \mathbf{E}\cdot\text{grad}C_a + \mu_a C_a \text{div}\mathbf{E} , \tag{38}$$

while for the cations,

$$\mathbf{v}\cdot\text{grad}C_c = D_c\Delta C_c - \mu_c \mathbf{E}\cdot\text{grad}C_c - \mu_c C_c \text{div}\mathbf{E} \tag{39}$$

by combining Eq. (38) and Eq. (39), and assuming the quasielectroneutrality condition ($z_a C_a \approx z_c C_c$, we note both C), we get

$$(D_c - D_a)\Delta C - (\mu_a + \mu_c)\mathbf{E}\cdot\text{grad}C - (\mu_a + \mu_c)C\,\text{div}\mathbf{E} = 0 . \tag{40}$$

We can use this to eliminate in Eq. (39) the terms containing $\mathbf{E}$, and end up with

$$\mathbf{v}\cdot\text{grad}C = D\Delta C , \tag{41}$$

where $D = (D_a\mu_c + D_c\mu_a)/(\mu_a + \mu_c)$. [Equation (41) can be considered as an equation of conservation of mass when taking into account the advective term.]

Now, let us consider only the point A which lies at the summit of the arch. A is a hyperbolic point for the fluid flow, as shown in Fig. 11. We can approximate the fluid flow, in the vicinity of A, by the flow $\mathbf{v}(x,y) = (ax)\mathbf{i} - (ay)\mathbf{j}$, where $\mathbf{i}$ is a normalized vector orthogonal to the teeth, and $\mathbf{j}$ a normalized vector parallel to the teeth, and $a = \partial\mathbf{v}\cdot\mathbf{i}/\partial x$. Then from Eq. (41), the concentration satisfies the following equation:

$$D\left[\frac{\partial^2 C}{\partial x^2} + \frac{\partial^2 C}{\partial y^2}\right] = (ax)\frac{\partial C}{\partial x} - (ay)\frac{\partial C}{\partial y} . \tag{42}$$

Let us call d the width of the transition zone between the concentrated and the emptied zones; we can approximate from Eq. (42)

$$DC/d^2 \approx ad(C/d) , \tag{43}$$

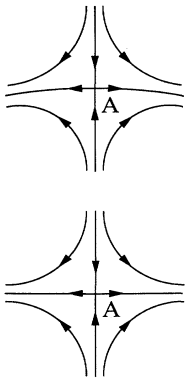

FIG. 11. Top: Scheme of the fluid flow in the vicinity of A, which is a stagnation point in the moving frame. Bottom: The linearized flow which allows one to determine the $D^{1/2}$ dependence of the width of the transition zone.

so finally

$$d \approx (D/a)^{1/2} . \tag{44}$$

There is a given value of a for each fluid pattern. Another way of understanding why d does not vary linearly with D is to realize that, as the ions diffuse more easily, they penetrate into regions (such as the inner parts of the vortices) where the fluid speed is larger. This in turn tends to sharpen the transition. The interplay of the smoothing effect (enlarging the diffusion constant) and of the sharpening effect (faster fluid speed) gives rise to a dependence of d which is proportional to the square root of $(D/|\nabla \mathbf{v}|)$.

Note that d will also depend on the distance to the tip, because the magnitude of $\mathbf{v}$ depends on the distance to the tip. While the absolute magnitude may change, the dependence on D will still be of the form $d \approx D^{1/2}$. Note also that the Péclet number vb/D varies along the arch, because the flow is not laminar.

Let us finally remark that, since the value of a in Eqs. (42)–(44) is of the order of

$$a \approx \mu_a |E_\infty| / b , \tag{45}$$

d will be of the order of

$$d \approx \left[\frac{Db}{\mu_a |E_\infty|} \right]^{1/2} \approx \left[\frac{kT}{e|E_\infty|} b \right]^{1/2} \approx (\lambda_b b)^{1/2} . \tag{46}$$

Since λ_b is smaller than b, d is also smaller than b.

As stated before, the case studied in Sec. IV is merely the limit for vanishing D of a more general problem, and in that limit, one should recover a steep archlike concentration step. We now proceed and present a simplified solution of the ECD process which includes convection, diffusion, and drift.

B. An approximation of the complete problem

We will not attempt to solve the whole set of equations (35)–(37). The Navier-Stokes equation is coupled to the electric equations in the charged zone only. Since this zone is expected to be very small we can consider the force inside this zone as a parameter and take the fluid flow as a fixed field whose shape is known analytically, once the force is known. With this hypothesis, one can rather easily find the concentration and potential field numerically.

We expect that the two concentration fields $z_c C_c$ and $z_a C_a$ will be almost identical in the QNR, again, we call them both C. As stated before, neutrality is a very good approximation in the QNR, and, as above, we consider the zone where a large excess of cations is found to be confined in a single point: the tip of the branches. Of course, we restrict ourselves to the steady state, and start again with Eqs. (38)–(41) coupled to Eq. (28), giving the fluid velocity at any point around the comb. Now, this is in fact a much simpler problem. By solving numerically Eq. (41), with the fixed fluid velocity given by Eq. (28), we will get the concentration map of both cations and anions. Knowing that the anions are frozen, we recover the shape of the electric field by means of

$$\mathbf{E} = (\mathbf{v} C_a - D_a \mathrm{grad} C_a)/\mu_a C_a . \tag{47}$$

The specific charge distribution Q inside the vortex, which will allow the electric field to have such a shape, will be given by

$$Q = \epsilon \epsilon_0 \mathrm{div} \mathbf{E} , \tag{48}$$

which can be expressed as a function of C alone:

$$Q = -\epsilon \epsilon_0 (D_a/\mu_a) \mathrm{div}[(\mathrm{grad} C)/C] . \tag{49}$$

Using Eq. (41), Q can be expressed in the following form:

$$Q = -\epsilon \epsilon_0 (D_a/\mu_a) \times [(1/D)(\mathbf{v} \cdot \mathrm{grad} C)/C - (\mathrm{grad} C)^2/(C)^2] . \tag{50}$$

(This form is more suitable, from a numerical point of view, because it makes use of only one derivative of C.)

C. Numerical solution of the simplified problem

We have solved Eqs. (41) and (28) numerically. We describe in the Appendix some technicalities of the numerical computation. We present here the results which were obtained with an explicit recursion scheme on a grid with discretization 82×160. We show in Fig. 12 a typical concentration map, in the region ahead of the vortices, for a value of α equal to 2, and a value $\mathcal{D} = 5 \times 10^{-3}$, where $\mathcal{D}$ is a parameter proportional to the ambipolar diffusion constant: $\mathcal{D} = (24\pi \rho v b/sf) D$. As expected from simple arguments, the transition zone is widened by diffusion. As $\mathcal{D}$ is decreased, the pattern gets closer to the solution which was first presented in Ref. [34] and further discussed in Sec. IV. When the diffusion constant is very large, the ions can penetrate between the teeth of the comb very efficiently, as if there were no fluid motion at all, thus the concentration pattern tends towards a purely diffusive one. We have checked that, in this limit, C is proportional to the Laplace potential between a comb and a linear anode.

FIG. 12. Typical concentration map as given by the computation ($\mathcal{D}=5\times10^{-3}$). The alternate black and white stripes correspond to $C_\infty/10$ concentration intervals. The concentration is set to zero in the rear part of the branches (see the Appendix). Tips are at the bottom corners of the picture.

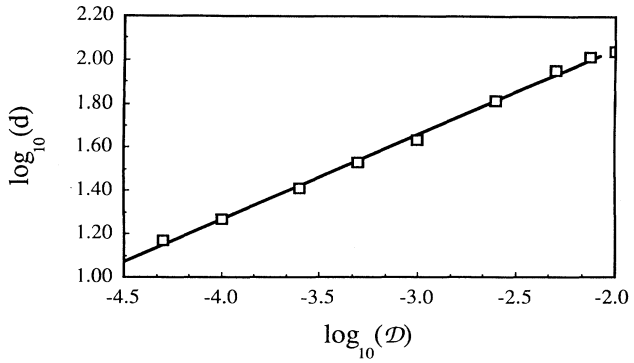

FIG. 14. Thickness d of the transition zone as a function of $\mathcal{D}$ (the thickness is measured as the length between the point where $C=0.1C_\infty$ and the point where $C=0.9C_\infty$, halfway between branches). The slope of the line, drawn through the calculated points, is here ~0.4.

In order to see how the concentration map goes from a solution similar to the Laplace potential between a comb and a linear anode, to the solution of Sec. IV, we have plotted the concentration profile halfway between two branches, as a function of $\mathcal{D}$ (Fig. 13). We have also plotted the thickness d of the transition zone as a function of $\mathcal{D}$ (Fig. 14). We find a power-law dependence, close to $\mathcal{D}^{1/2}$. Note that for larger values of $\mathcal{D}$ it saturates to the size of the cell, which is sensible. Of course, one expects the thickness of the transition zone to vary with the position along the arch, as stated before. Then the behavior depicted in Fig. 9 catches the main features of the motion of the ions, except that diffusion will spread the otherwise sharp interface over a distance proportional to $D^{1/2}$.

The electric-field lines which we have derived numerically are shown in Fig. 15 for some values of $\mathcal{D}$. An associated distribution of charges, as deduced from Eq. (50), appears along the arch. As expected, in the limit of small $\mathcal{D}$, we recover a field proportional to the fluid speed, associated with a distribution of charges more and more confined to the arch.

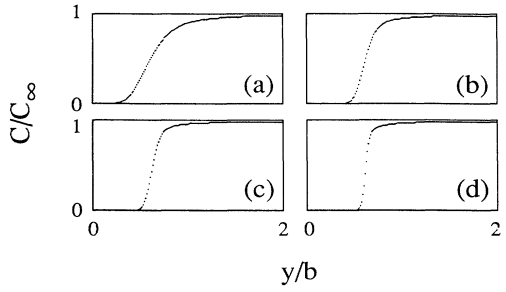

FIG. 13. One-dimensional cut through the concentration map, halfway between the two teeth: (a) $\mathcal{D}=5\times10^{-3}$, (b) $\mathcal{D}=10^{-3}$, (c) $\mathcal{D}=5\times10^{-4}$, (d) $\mathcal{D}=10^{-4}$. One notices that the concentration profile gets closer to the solution corresponding to Fig. 9, while $\mathcal{D}$ decreases. In the limit of large $\mathcal{D}$, one recovers a purely diffusive solution.

VI. EXPERIMENT

We have observed the growth of copper deposits in conditions which allow us to clearly see the arches ahead of the tips. This is the subject of the first subsection. In the second subsection we focus on the fluid motion, which we have been able to visualize with oil droplets used as tracers: The convective vortices are proved to exist. We then describe how branching and screening occur. Finally, we discuss some quantitative estimates which can be derived from these experiments.

A. Experiment using interferential contrast

We have used a Nikon Optiphot microscope equipped with a Nomarski interference-contrast accessory. This is

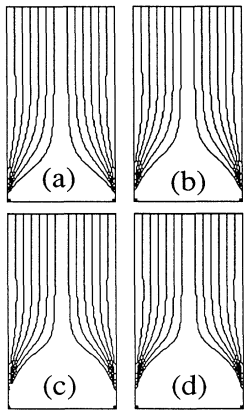

FIG. 15. The electric-field lines which are obtained from Eq. (47) (see text). (a) $\mathcal{D}=10^{-2}$, (b) $\mathcal{D}=5\times10^{-3}$, (c) $\mathcal{D}=10^{-3}$, (d) $\mathcal{D}=5\times10^{-4}$. As explained in Fig. 10, this peculiar shape of the field is not the one expected between a comb and a linear anode. Since the motion of the ions is only governed by diffusion, drift, and convection, the model predicts that, in the steady state, there will be a specific distribution of charges, in order for the field to have such a shape.

used traditionally by metallurgists in order to detect scratches or small irregularities on metal surfaces. It is also used by biologists in order to distinguish microscopic details of bacteria or other cells, which are usually transparent, but whose refractive index is not the same as water. The principle of the interferometric contrast is the following. The beam produced by a source of light passes first through a birefringent prism. The two polarities of the light are slightly separated into two beams. Suppose the sample is a transparent object, of nonuniform refractive index, there will be a difference between the optical paths of the two beams. If now the two beams interfere before coming back to the eyepiece, it results in a shadowed picture of the refractive-index map, mimicking a relief under grazing illumination. In our case, the difference in optical path will be due to the differences in refractive index, because of the concentration gradients. The setup is as described in Fig. 16. A small electrochemical cell (1 cm$\times$1.5 cm$\times$0.1 mm) is placed on the sample holder of the microscope. This cell consists of two microscope cover plates glued to two parallel copper stripes acting as the electrodes. The lower plate is metallized on its lower side, so it works as a mirror. The cell is filled with a solution of copper sulphate by means of capillarity through the sides, which remain open. The two light beams, after being separated by the refractive prism, cross the upper glass plate (thickness 0.16 mm), cross the solution, then the lower glass plate, are reflected on the lower side of the glass plate, and come all along the way back. In the end, they form the contrasted image in the eyepieces. As one notices, the solution is crossed twice, and the glass plates are crossed four times. Calibration tests showed that the thickness of the glass plate was not critical. However, the thickness of the layer of solution had to be chosen below 0.2 mm in order to obtain a good contrast.

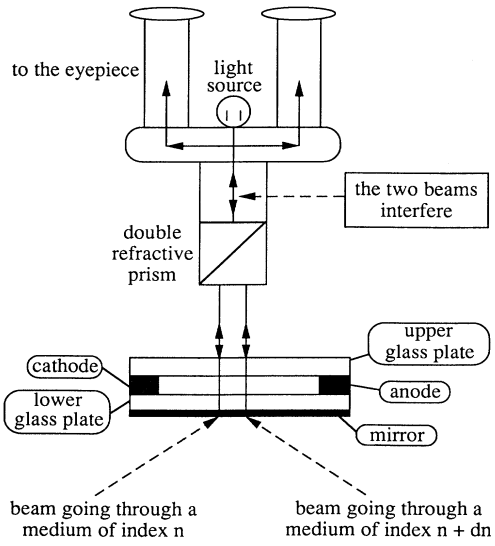

FIG. 16. Sketch of the experimental setup. The Nomarski interferential contrast gives a shadow image of the concentration profile.

The experiments which we report on here were carried out with solutions of copper sulphate in the range 5×10^{-3} moll^{-1} to 8×10^{-2} moll^{-1}, i.e., sufficiently small so that the independent-ion approximation is not too bad, and sufficiently large that the optical contrast is high enough.

For practical purposes we used a potential generator. The applied potential was in the interval 2–15 V. However, we checked with a current generator that the growth, in the same range of initial potential, is of the same kind and exhibits the same features. The duration of a typical growth, in these conditions, is between 1 and 10 min (for example, with 2×10^{-2} moll^{-1} and 15 V, the growth lasts 2 min).

We show in Fig. 17 two typical images that we obtained. There is an interval of a few seconds between the two snapshots. As one notices, the concentration step is not perfectly sharp; however, as predicted from the model, the transition zone is shaped like an arch. In order to compare the experimental shape to the theoretical one, we show in Fig. 18 the concentration gradients, as obtained from Fig. 12. The comparison shows that the experiment is near the limit of small D. This will be discussed in the last part of this section.

We have also observed that, for large currents (some tens of mA/cm^2), there is a very active competition between the arches, which corresponds to a very active competition between the vortices. For very large currents one can hardly speak of vortices, and the motion of the liquid is turbulent in front of the branches, but the flow is still inwards, and shaped like a funnel at the active tips.

B. Observation of the convective vortices

Several attempts were made in order to see the convective vortices with different powders and tracers. The

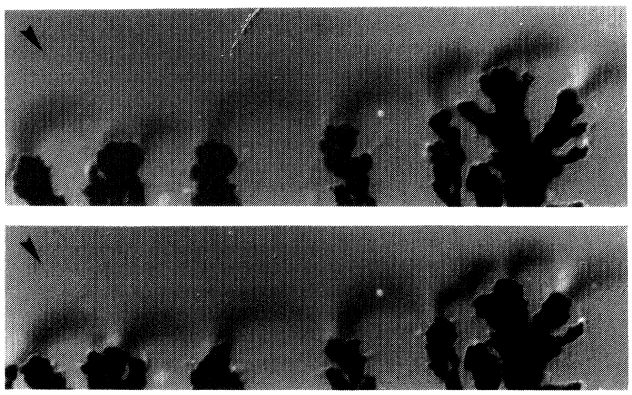

FIG. 17. Two consecutive images of the concentration gradient obtained with the interferential contrast (see text) on an almost steady growth. One should view the contrast on the pictures as the shadow of the concentration profile, with a spot light coming from the direction of the arrow. The concentration is 5×10^{-2} moll^{-1}, a potential of 8 V was applied, the cell geometry is 0.1 mm$\times$1 cm$\times$1.5 cm (because of using constant potential in this experiment, the growth is not in the steady state).

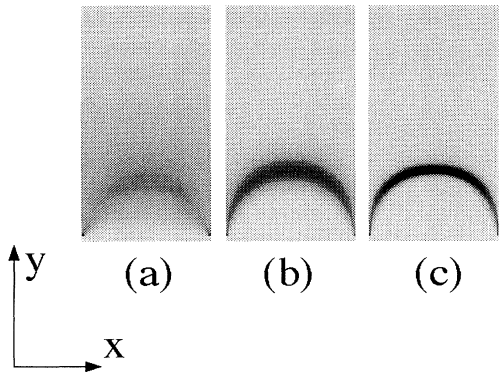

FIG. 18. Maps of $\partial C/\partial y$, for the values of $\mathcal{D}$ which give concentration maps comparable to the experimental case. The maps are shown over the same region of the cell as in Fig. 12. (a) $\mathcal{D}=10^{-2}$, (b) $\mathcal{D}=10^{-3}$, (c) $\mathcal{D}=10^{-4}$.

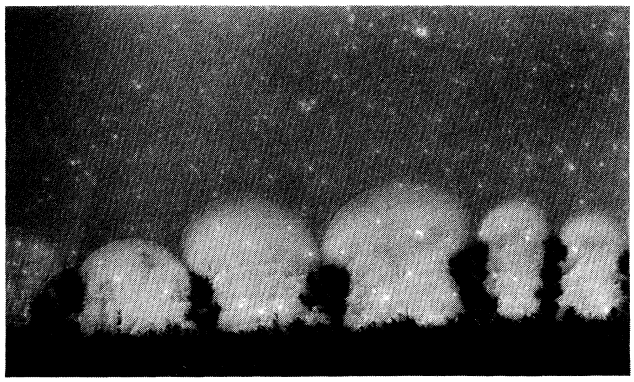

FIG. 19. Image of the convective vortices, just after the beginning of the growth. The darker aspect of the upper part of the picture is due to the very small oil droplets (diameter ≈ 1 μm) which are in the solution. The droplets hardly penetrate below the arch, because the fluid flow makes them drift through the funnel. (Same experimental conditions as in Fig. 17.) Note that the feet of the arches, where the tips are located, are very narrow: these are very active zones due to the high speed of the liquid going inwards.

reason why it has proved hard to find a good tracer is that, as appears in Fig. 8, all the liquid goes once through the tip. This means that whatever the tracer one puts in the electrolyte, it will all end up at the tip. This could explain in part why the deposit is very sensitive to any impurity present in the solution. However, we found it very satisfactory to add a very small amount of Esso cutwell 40 oil to the solution. In the case we report on here, we diluted one drop of oil in 100 cm^3 of copper sulphate electrolyte. The oil split into many very small droplets (1–10 μm), forming a milky emulsion with water. The emulsion is rather stable over three days. Such a dilute emulsion permitted us to see the vortices without hindering growth. However, growth was slightly disturbed by the oil. One must also keep in mind that the shape of the vortices depends on the viscosity of the solution. Adding a drop of oil certainly does change the viscosity of the solution. However, while this effect was not controlled, it did not seem to affect the patterns very much. The same solutions of copper sulphate, with concentrations ranging from 5×10^{-3} mol l^{-1} to 8×10^{-2} mol l^{-1} were used, and the values of the applied potential also ranged between 2 and 15 V. The electrochemical cell is similar to the one described above. We show a typical picture in Fig. 19. We could not see the concentration gradients together with the vortices because the small oil droplets diffuse light. The vortices were observed, and their motion was recorded with a charged-coupled-device (CCD) camera at different magnifications (50×, 100×, and 200×). Their features do correspond to the predicted ones. Namely, two contrarotative vortices are *always* found between two neighboring active branches, in the dense parallel regime, in the range of parameters which we have studied. The vortices are found just below an arch. As a matter of fact, the part ahead of the vortices could be better seen for the following reason: The water that enters the inner part of the vortices below the arch has gone through the deposit. Therefore, it contains less droplets, because the oil seems to stick to the deposit, though it does not hinder the growth. However, the droplets and some powdery copper (coming from the deposit) which enter the vortices are largely sufficient to see the motion of the fluid. Without a doubt, the simple observations that we report here rule out any model of growth in similar conditions which would not take into account hydrodynamics. Let us repeat that the arches which appear in Fig. 19 are not due to concentration gradients. They show where tracers are found and where they are not. The arch is very sharp because there is no diffusion of the tracers. The overall shape of the vortices and of the fluid flow seems to be rather well described by the simple model that we have presented in the preceding sections.

It is revealed from the pictures that the funnels are very sharp at the tips. This shows that the approximation of very thin needles is very good, though the branches themselves are thick. Also, the volume on which the force acts does not encompass the tips on all their width, as it could have been naively expected. It seems that, after passing through the funnel, the solution moves turbulently through the branch, which is much thicker than the funnel; growth can then occur inside the growing branch, a few tens of microns behind the tips. Also, the fluid velocity is very large at the tips, thus provoking the observed shaking of the active zone. Obviously, the fluid flow is also three dimensional and turbulent when the distance between branches is small.

We also noticed that there is a global and quite slow motion of the tracers towards the anode. This can be due to an electrophoretic effect [38]. However, it is so slow that it does not change deeply the fluid pattern.

We also observed that when the deposit arrives at the other end of the cell, near the anode, the vortices which we have described previously disappear. The deposit stops a few tenths of millimeter afar from the anode and starts to thicken. When the deposit stops, another kind of convective motion sets in. One or two cylindrical rolls appear between the anode and the deposit. These

cylinders lie parallel to the anode, and are certainly linked to buoyancy. We will not discuss this effect any further here.

C. Observation of branching and screening

We have been able to observe branching and screening quite easily. We have seen with interferential contrast that, when a tip splits, an arch joining the two baby branches appears. Also, we have observed the slow vanishing of an arch when a branch is screened and "dies." These patternings of the deposit proceed concomitantly with the formation and vanishing of pairs of contrarotative vortices between neighboring branches, which can be observed because of very small impurities which are still present in the solution. The formation and vanishing of pairs of contrarotative vortices was evident with the oil droplets (see Fig. 20), but, as stated before, we could not observe the concentration and the droplets in the same experiment.

D. The beginning of the growth

The understanding of the beginning of the growth is of upmost importance in order to fully understand the growth itself. Hence, we have carefully observed the first stages of the growth. At the very beginning of the growth (up to 10 s or so, depending on the experimental conditions), one observes under interferential contrast that a more contrasted layer forms near the cathode. (The liquid is at rest at this stage.) This means that a zone of different chemical conditions builds along the smooth cathode. This zone corresponds to the depleted zone of Chazalviel's model; this will be described in detail elsewhere [25]. After this first stage, one observes a complicated turbulent motion of the fluid near the electrode, on a scale of order 1 mm. Though the flow is turbulent, there is a general trend of the fluid motion, which consists in making three-dimensional whirls which bring the solution near the electrode and then away from the electrode. These whirls can be seen with the oil-droplet method. When watching under interferential contrast one sees many small arches that compete and have a wavy unsteady behavior, which is linked to the underlying motion of the fluid. During this stage of the electrodeposition process, the deposit is very small, smaller, in fact, than the cell thickness. This random motion of the fluid, and of the concentration arches, organizes itself progressively, until the large steadier vortices finally appear. It seems that as soon as the vortices are formed, larger branches at the feet of the arches exist. However, it is hard to tell, from the above observations, whether the branches organize the vortices, or the converse. We should emphasize the interesting fact that, in some instances, when branches are too fragile, the vortices do exist, though the branches were destroyed as they grew. This is especially the case when very large currents are employed.

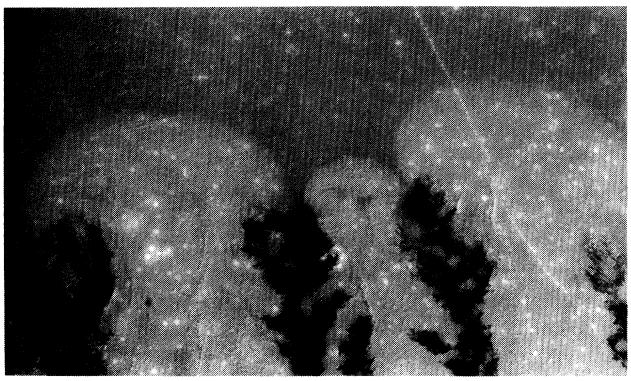

FIG. 20. The convective vortices, in the vicinity of two tips which are getting closer. The vortices still exist, but become all the smaller as the distance between the branches gets smaller. Eventually, a pair of small vortices will disappear and one of the branches will survive.

E. Quantitative aspects

One can notice in the pictures of the concentration gradients and of the vortices that, while the distance between trees is not constant, due to the particularities of the deposit, the aspect ratio of the arch is roughly the same and of the order of unity (this is particularly clear in Fig. 17). This means that point A, where the fluid velocity is zero, stands always at coordinates $(b/2,h)$, with $h \approx b/2$ ($x=0$ is on a branch). This gives an experimental estimate of the force which acts at the tip of the branches. Indeed, since $\mathbf{v}(A)=\mathbf{0}$, we must have $\mathrm{curl}\Psi(A)=0$. This condition implies that

$$-\mu_a E_\infty + \frac{s}{24\pi\rho\nu} f \partial_x \left[\sum_{k=-\infty}^{k=+\infty} \frac{x-kb}{r_k^2} \right]_{\substack{x=b/2 \\ y=b/2}} = 0 , \tag{51}$$

or,

$$-\mu_a E_\infty + \frac{s}{24\pi\rho\nu(b/2)^2} f \sum_{k=-\infty}^{k=+\infty} \frac{1-(1-2k)^2}{[1+(1-2k)^2]^2} = 0 . \tag{52}$$

This gives an estimated value f_e for the force f:

$$f_e \approx \mu_a E_\infty [15\pi\rho\nu b^2/s] . \tag{53}$$

A numerical estimate of f_e, with $\mu_a = 8.64\times10^{-4}$ $\mathrm{cm^2\,V^{-1}\,s^{-1}}$, $E_\infty = 10$ V/cm, $\rho = 10^3$ $\mathrm{kg\,m^{-3}}$, $\nu = 10^{-2}$ $\mathrm{cm^2\,s^{-1}}$, $b = 5\times10^{-2}$ cm, $s = 10^{-2}$ cm, gives $f_e \approx 10^{-8}$ N. We have also shown in Sec. III that, because of flux conservation, the electric force f that exists on top of a branch when the fluid is at rest is given by Eq. (25). A numerical estimate of f, with the same values as above, and $C_c = 10^{-2}$ $\mathrm{mol\,l^{-1}}$, $z_c = 2$, $\mu_c = 5.76\times10^{-4}$ $\mathrm{cm^2\,V^{-1}\,s^{-1}}$, $x_1 \approx 10^{-6}$ m, gives $f \approx 10^{-4}$ N. These estimates show that, in principle, the electric force at the tip is 10^4 times larger than what is required in order to provoke a convective motion like the observed one. Of course, one must keep in mind that the value of f has been derived in the case of a steady fluid: As soon as the convective motion has set in, the calculation is no longer

valid. Especially, the charged zone will extend over a very narrow region close to the dendrites in which boundary layer effects must be taken into account. Also, the branches hinder the motion of the fluid, and a full description of the turbulent zone, including friction inside the tip, would certainly lead to a much lower value of the force which is available for the convective motion between the teeth.

Let us also add the following result concerning the value of the diffusion constant. Taking into account the previous results, ψ is written as

$$\psi \approx b v_a \left[\frac{x}{b} + \frac{15}{24} \sum_{k=-\infty}^{k=+\infty} \frac{\frac{x}{b} - k}{\left[\frac{r_k}{b} \right]^2} \right] . \tag{54}$$

The value of the numerical parameter $\mathcal{D}$ which is observed seems to be close to 10^{-2}. Since $D \approx b v_a \mathcal{D}$, $b \approx 10^{-1}$ cm, and $v_a \approx 10^{-2}$ cm s^{-1}, we derive $D \approx 10^{-5}$ cm^2 s^{-1}, which is very close to the known value of the ambipolar diffusion constant in $CuSO_4$.

VII. CONCLUSION

We have presented a model which, in our opinion, catches the main features of the electrochemical aspects of the growth mechanism, in the dense parallel regime. This model incorporates electric drift, diffusion, and electroconvective motion. We have shown experimentally that the fluid flow and concentration maps around the deposit compare well with the predicted ones. We have proved experimentally, and conjectured on some simple arguments, that the convective vortices do not allow penetration of the solution between the branches in the steady-state regime. The observations and the theoretical model that we have presented rule out any model of ECD in similar conditions which would not take into account convection. In particular, the attempts to link the type of growth discussed here to diffusion limited aggregation seem rather questionable. This remark may not apply to growths in supported electrolyte or to growths at very low growth speeds, where diffusion is dominant over electric drift, and convection is weak. Let us remark however, that there is no onset to the convective motion, and that the speed of the fluid seems simply to decrease when the imposed current density is decreased. Also, in the case where convection is suppressed [39], like in Hibbert and Melrose [12,13] experiments, our model may not hold (still, the model proposed by Chazalviel [22] for a steady solution may be valid). Also, preliminary experiments with zinc showed that convection is equally important around zinc deposits. The vortices are very similar to the ones observed in the case of copper sulphate, when the growth is in the dense parallel regime. The arches exist and their main features are analogous to the case of copper. However, in the case of needlelike crystalline dendrites large vortices between neighboring tips do not exist any longer. In this case, the active zone extends rather far behind the tip (several times the tip width) and some smaller vortices still exist, along the active sides of the dendrite. Note that, in this case, the boundary conditions near the dendrite are clearly not represented by a rectilinear comb. Also, the anisotropy favors so much the direction of growth that one can hardly achieve, in practice, a stationary state, and the vortices seem to correspond to the ones shown in Figs. 7(c) and 7(d) rather than 7(a) and 7(b), hence there is no arch between neighboring dendrites. A more detailed report on the case of zinc will appear later.

Finally, let us remark that when the current is switched off, the convective vortices are frozen almost at once. However, the arches of concentration still exist for a while, and slowly fade away. In our opinion, this rules out the Marangoni convection which has been conjectured [21,40] to possibly exist between the concentrated and nonconcentrated solution, due to the mismatch in surface tensions. Also, the shapes of the concentration gradients in these references are not the same as the ones we present here. One should notice two differences between the regime studied here and the one described by Barkey [21]. First, the zinc aggregates he obtains at low concentration are more compact than ours (Fig. 2 of Ref. [21(b)], for example), so it seems that the branches are too close to each other to allow the presence of vortices between them. On the other hand [Fig. 6 of Ref. [21(b)]] in the case of well-separated branches (dendritic growth) a parabolic envelope is found around the dendrites which does not resemble the arches we present here. But it should be noticed that, in this instance, very high concentrations are used ($0.2M$). We believe that natural convection provokes a gravity current [41] near the branches which gives rise to this envelope.

ACKNOWLEDGMENTS

This work was supported by the Centre National d'Etudes Spatiales under Contract No. 1989/1229. The Laboratoire de Physique de la Matière Condensée is "Unité de Recherche Associée No. 1254" of the Centre National de la Recherche Scientifique. V.F. acknowledges fruitful discussions with Olivier Pouliquen and Jean-François Chomaz of the Laboratoire d'Hydrodynamique de l'Ecole Polytechnique on Navier-Stokes Equation, and with Touffic Aboud of the Laboratoire de Mathématiques Appliquées de l'Ecole Polytechnique on numerical calculations. Also, V.F. is grateful to Françoise Argoul for sharing results on gravity-driven convection prior to publication.

APPENDIX

We describe in this appendix some technical aspects of the numerical calculation.

The concentration map C was computed on a VAX 9000 computer. We have in fact used two grids, one of size 42×160 and one of size 82×160. We have found it necessary to take a rather elongated cell, so that the concentration gradients, which are expected to extend over a length (at most) of the order of the distance between teeth, would not be too sensitive to the presence of the cathode and of the anode. Since the speed is in principle infinite at the tips, we introduced a cutoff around the tips.

Namely, the concentration was set to zero not on the tip itself but on a neighborhood of two pixels (respectively, five pixels) around the tips in the case of the smaller grid (respectively, in the case of the larger grid). An explicit recursion scheme was used:

$$[C^{k+1}(i,j)-C^k(i,j)]/dt = \mathcal{D}[C^k(i+1,j)+C^k(i-1,j)+C^k(i,j+1)+C^k(i,j-1)-4C^k(i,j)] - v_x(i,j)\delta_x^k(i,j)-v_y(i,j)\delta_y^k(i,j)\ , \quad \text{(A1)}$$

where

$$\delta_x^k(i,j)=\begin{cases}[C^k(i+1,j)-C^k(i,j)] & \text{if } v_x(i,j)<0 \quad \text{(A2a)}\\ [C^k(i,j)-C^k(i-1,j)] & \text{if } v_x(i,j)>0 \quad \text{(A2b)}\end{cases}$$

and

$$\delta_y^k(i,j)=\begin{cases}[C^k(i,j+1)-C^k(i,j)] & \text{if } v_y(i,j)<0 \quad \text{(A3a)}\\ [C^k(i,j)-C^k(i,j-1)] & \text{if } v_y(i,j)>0\ . \quad \text{(A3b)}\end{cases}$$

We use for $\mathbf{v}$ the curl of the vector $(0,0,\psi_\alpha)$ with ψ_α:

$$\psi_\alpha=\alpha\frac{x}{b}+\sum_{k=-\infty}^{k=+\infty}\frac{\frac{x}{b}-k}{\left[\frac{r_k}{b}\right]^2} \quad \text{(A4)}$$

(where b is the width of the box in lattice units).

So, the fluid velocity was given by

$$v_x(i,j)=\psi_\alpha(i,j+1)-\psi_\alpha(i,j)\ , \quad \text{(A5)}$$

$$v_y(i,j)=\psi_\alpha(i,j)-\psi_\alpha(i+1,j)\ . \quad \text{(A6)}$$

We have explored different values of fluid speeds (hence different values of α). We then focused on fields corresponding to $\alpha=0.25$ and $\alpha=2$ [which is the fluid flow shown in Fig. 7(b)]. We started from a purely diffusive concentration map (i.e., Laplacian potential), and a high diffusion constant. We used as the control parameter the parameter $\mathcal{D}$, which is related to the true ambipolar diffusion constant D by

$$D=(sf/24\pi\rho\nu b)\mathcal{D} \quad \text{(A7)}$$

(where b is the distance between branches in the real experiment). Let us insist on the fact that the conditions (A2) and (A3) arise because of convergence problems when the gradient is not taken in the direction of the flow. As a matter of fact, this condition is not absolutely necessary when the diffusion constant is large, but convergence becomes more and more difficult as the diffusion constant is lowered. It should be noticed that the fluid velocity is very large at the tips. When the diffusion constant is decreased, the advective term starts playing a greater role, and the transition zone sharpens. This means that the $\mathbf{v}\cdot\nabla C$ term becomes larger in a nonlinear way [much like in Navier-Stokes equations with large Reynolds numbers, of which Eq. (41) is a scalar analog]. This causes a rapid divergence of the algorithm, which is always triggered at the tips, if conditions (A2) and (A3) are not implemented. In order to achieve good accuracy and rapid convergence, we proceeded in the following way. The solution with one value of $\mathcal{D}$ was used as input for the next computation with smaller $\mathcal{D}$. It would take typically 10 000 iterations to reach convergence for values of $\mathcal{D}$ in the range 10^{-4}–10^{-1}. In fact, though D and dt must satisfy $dt\mathcal{D}\leq 1$ in order to ensure convergence for the calculation of the Laplace potential, we found it possible to loosen this condition, in the case of the equation we are discussing here, Eq. (41), while the diffusion constant was decreased. For values of $\mathcal{D}$ in the range 2.5×10^{-4}–10^{-2} we could go up to $\mathcal{D}dt=10$. Also, in order to ensure reasonable resolution, we have chosen to use a rather coarse grid of size 42×160, with teeth of length 80 along the larger side for values of $\mathcal{D}$ above 10^{-3}. Below this value of $\mathcal{D}$, the concentration between the teeth is lower than 0.02. We then imposed $C=0$ between the teeth, and restricted the computation to a smaller box corresponding to the zone ahead of the branches. We could use in this box a finer grid, of size 82×160. As a matter of fact, the use of a smaller box, with a concentration equal to zero in between the branches, does not lead to a pattern which matches exactly the pattern calculated in the larger box (keep in mind that the discretization is *better* in the small box). However, the discrepancy is very small, and can be neglected, in a first approximation. A refinement would be to take the values of the concentration determined with the coarse grid as the new boundary condition between the tips.

[1] T. A. Witten and L. M. Sander, Phys. Rev. Lett. **47**, 1400 (1981).

[2] T. A. Witten and L. M. Sander, Phys. Rev. B **27**, 5686 (1983).

[3] M. Matsushita, M. Sano, Y. Hayakawa, H. Honjo, and Y. Sawada, Phys. Rev. Lett. **53**, 286 (1984).

[4] D. Grier, E. Ben-Jacob, R. Clarke, and L. M. Sander, Phys. Rev. Lett. **56**, 1264 (1986).

[5] Y. Sawada, A. Dougherty, and J. P. Gollub, Phys. Rev. Lett. **56**, 1260 (1986).

[6] D. G. Grier, D. A. Kessler, and L. M. Sander, Phys. Rev. Lett. **59**, 2315 (1987).

[7] M. K. Pon and L. Lam, in *Nonlinear and Chaotic Phenomena,* edited by W. Rozmus and J. A. Tuszynski (World Scientific, Teaneck, NJ, 1991).

[8] F. Argoul, A. Arneodo, G. Grasseau, and H. L. Swinney, Phys. Rev. Lett. **61**, 2558 (1988).

[9] Y. Sawada and H. Hyosu, in *Fractals in Physics,* Proceedings of the International Conference on honoring Benoît B. Mandelbrot on his 65th birthday, edited by A. Aharony and J. Feder (North-Holland, Amsterdam, 1989) [Physica D **38**, 299 (1989)].

[10] P. Garik, D. Barkey, E. Ben-Jacob, E. Bochner, N. Broxholm, B. Miller, B. Orr, and R. Zamir, Phys. Rev. Lett. **62**, 2703 (1989).

[11] J. R. Melrose, D. B. Hibbert, and R. C. Ball, Phys. Rev.

Lett. **65**, 3009 (1990).
[12] D. B. Hibbert and J. R. Melrose, Phys. Rev. A **38**, 1036 (1988).
[13] D. B. Hibbert and J. R. Melrose, Proc. R. Soc. London Ser. A **423**, 149 (1989).
[14] G. L. M. K. S. Kahanda and M. Tomkiewicz, J. Electrochem. Soc. **136**, 1497 (1989).
[15] L. Lam, R. D. Pochy, and V. M. Castillo, in *Nonlinear Structures in Physical Systems,* edited by L. Lam and H. C. Morris (Springer, New York, 1990).
[16] V. Fleury, J.-N. Chazalviel, M. Rosso, and B. Sapoval, J. Electroanal. Chem. **290**, 249 (1990).
[17] V. Fleury, M. Rosso, and J.-N. Chazalviel, Phys. Rev. A **43**, 6908 (1991).
[18] V. Fleury, J. Mater. Res. **6**, 1169 (1991).
[19] V. Fleury, M. Rosso, J.-N. Chazalviel, and B. Sapoval, Phys. Rev. A **44**, 6693 (1991).
[20] R. H. Cork, D. C. Pritchard, and W. Y. Tam, Phys. Rev. A **44**, 6940 (1991).
[21] (a) D. Barkey and P. D. Laporte, J. Electrochem. Soc. **137**, 1655 (1990); (b) D. Barkey, *ibid.* **138**, 2912 (1991).
[22] J.-N. Chazalviel, Phys. Rev. A **42**, 7355 (1990).
[23] R. Bruinsma and S. Alexander, J. Chem. Phys. **92**, 3074 (1990).
[24] M. Rosso, J.-N. Chazalviel, and V. Fleury, in *Growth Patterns in Physical Systems and Biology,* edited by E. Louis, L. Sander, and P. Meakin (Plenum, New York, in press).
[25] M. Rosso, E. Chassaing, J.-N. Chazalviel, V. Fleury, and I. Solomon (unpublished).
[26] P. Atten and R. Moreau, J. Méc. (France) **11**, 471 (1972).
[27] Makoto Suzuki, Phys. Rev. A **31**, 2548 (1985).
[28] M. J. Gross and J. E. Porter, Nature (London) **17**, 1343 (1966).
[29] D. Avsec and M. Luntz, C. R. Acad. Sci. (Paris) **203**, 1140 (1936); **204**, 420 (1937); **204**, 757 (1937).
[30] R. J. Turnbull, Phys. Fluids **11**, 2588 (1968).
[31] J. M. Schneider and P. K. Watson, Phys. Fluids **13**, 1948 (1970).
[32] E. J. Hopfinger and J. P. Gosse, Phys. Fluids **14**, 1671 (1971).
[33] A. P. Grygin, Magnet. Hydrodynamica (Acad. Sci. of Latvia, Riga) **1**, 103 (1990); Electrokhimiya (Sov. Phys., Acad. Sci. SSSR, Moskow) **22**, 1457 (1986).
[34] V. Fleury, J.-N. Chazalviel, and M. Rosso, Phys. Rev. Lett. **68**, 2492 (1992).
[35] L. Landau and E. Lifschitz, *Fluid Mechanics* (Mir, Moscow, 1984).
[36] The force term f on p. 2493 of Ref. [34] has actually dimensions of (force)$\times$(length) and should be replaced by f/s.
[37] On p. 2494 of Ref. [34] a typing error has turned the word "connected" into "convex."
[38] According to F. Argoul (private communication) it is due to natural convection. While completing this paper, we did experiments with larger concentrations (1 $\mathrm{mol\,l^{-1}}$) which support Argoul's suggestion. However, the effect of gravity seems weak, for concentrations $C<5\times10^{-2}$ $\mathrm{mol\,l^{-1}}$.
[39] Electroconvection, as seen under the microscope, is such a violent effect that we would not be surprised if filter paper would not be enough to suppress it.
[40] P. Garik, J. Hetrick, B. Orr, D. Barkey, and E. Ben-Jacob, Phys. Rev. Lett. **66**, 1606 (1991); D. Barkey, P. Garik, E. Ben-Jacob, B. Miller, and B. Orr, J. Electrochem. Soc. **139**, 1044 (1992). See also D. Barkey, *Extended Abstracts of the 181st Meeting of the Electrochemical Society, St. Louis, MO, 1992* (Electrochemical Society, New York, 1992), Vol. 92, p. 499.
[41] John E. Simpson, *Gravity Currents in the Environment and in the Laboratory* (Ellis Horwood, Chichester, England, 1987).

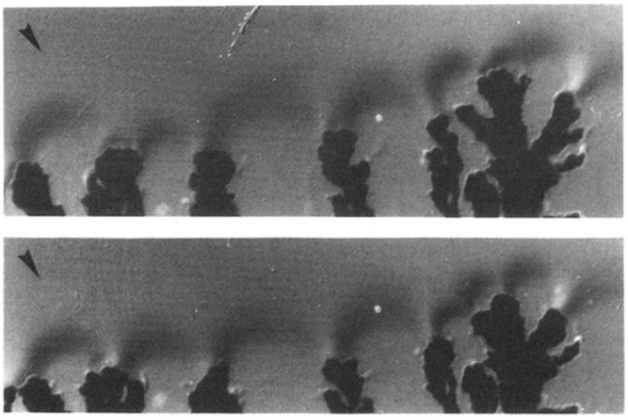

FIG. 17. Two consecutive images of the concentration gradient obtained with the interferential contrast (see text) on an almost steady growth. One should view the contrast on the pictures as the shadow of the concentration profile, with a spot light coming from the direction of the arrow. The concentration is 5×10^{-2} mol l^{-1}, a potential of 8 V was applied, the cell geometry is 0.1 mm $\times$ 1 cm $\times$ 1.5 cm (because of using constant potential in this experiment, the growth is not in the steady state).

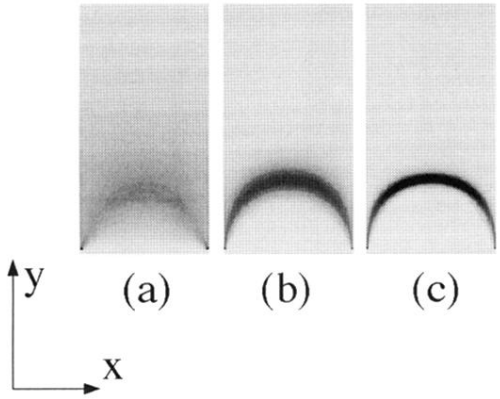

FIG. 18. Maps of $\partial C/\partial y$, for the values of $\mathcal{D}$ which give concentration maps comparable to the experimental case. The maps are shown over the same region of the cell as in Fig. 12. (a) $\mathcal{D}=10^{-2}$, (b) $\mathcal{D}=10^{-3}$, (c) $\mathcal{D}=10^{-4}$.

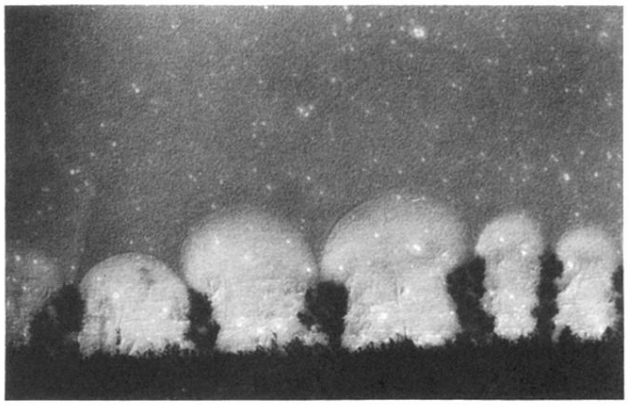

FIG. 19. Image of the convective vortices, just after the beginning of the growth. The darker aspect of the upper part of the picture is due to the very small oil droplets (diameter ≈ 1 μm) which are in the solution. The droplets hardly penetrate below the arch, because the fluid flow makes them drift through the funnel. (Same experimental conditions as in Fig. 17.) Note that the feet of the arches, where the tips are located, are very narrow: these are very active zones due to the high speed of the liquid going inwards.

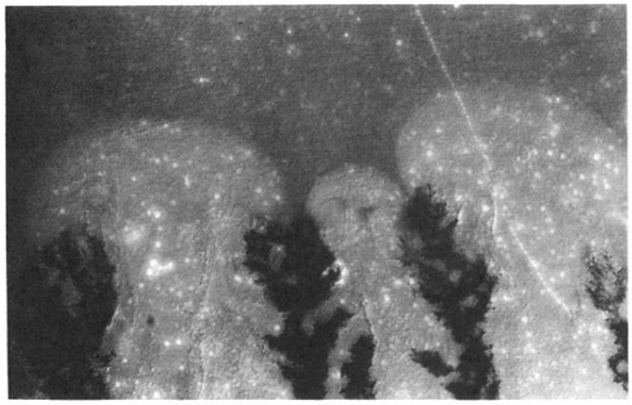

FIG. 20. The convective vortices, in the vicinity of two tips which are getting closer. The vortices still exist, but become all the smaller as the distance between the branches gets smaller. Eventually, a pair of small vortices will disappear and one of the branches will survive.